

# Computational Analysis of Supersonic Combustion Using Wedge-Shaped Strut Injector with Turbulent Non-Premixed Combustion Model

S. Roga, K. M. Pandey, A. P. Singh

**Abstract:-** This paper presents the supersonic combustion of hydrogen using wedge-shaped strut injector with two-dimensional turbulent non-premixed combustion model. The present model is based on the standard  $k$ -epsilon (two equations) with standard wall functions which is P1 radiation model. In this process, a PDF (Probability Density Function) approach is created and this method needs solution to a high dimensional PDF transport equation. As the combustion of hydrogen fuel is injected from the wedge-shaped strut injector, it is successfully used to model the turbulent reacting flow field. It is observed from the present work that, the maximum temperature occurred in the recirculation areas which is produced due to shock wave-expansion and the fuel jet losses concentration and after passing successively through such areas, temperature decreased slightly along the axis. From the maximum mass fraction of OH, it is observed that there is very little amount of OH around 0.0027 were found out after combustion. By providing wedge-shaped strut injector, expansion wave is created which cause the proper mixing between the fuels and air which results in complete combustion.

**Index Terms:-** CFD, combustion, hydrogen fuel, non-premixed combustion, scramjet, standard  $k$ -epsilon turbulence model, standard wall functions, steady state, supersonic combustion, two-dimensional, wedge-shaped strut injector.

## I. INTRODUCTION

Supersonic combustion ramjet (scramjet) is the key enabling technology for endure hypersonic flights. In the present scramjet engines the combustor length is generally of the order of 1 m and the residence time of the mixture is of the order of milliseconds. Problems occur in the mixing of the reactants, flame stability and completion of the combustion within the limited combustor length which occurs due to high speed of the supersonic flow in the combustion chamber. The flow field in the scramjet combustor is highly complex which shows that when the flight speed is low, the kinetic energy of the air is not enough to be used for the optimal compression. Further compression

by machines is required in order to obtain a higher efficiency. In a supersonic combustion ramjet or scramjet, the flow is compressed and decelerated using a series of oblique shock waves. A scramjet engine is well known as hypersonic air-breathing engine in which heat release due to combustion process, occurs in the supersonic flow relative to the engine. Therefore, the flow velocity throughout the scramjet remains supersonic and thereby it does not require mechanical choking system [1]. The scramjet propulsion system consists of the forebody, internal inlet, isolator, combustor, internal nozzle, aftbody and fuel supply subsystem [2].

Scramjet combustor advances from the better performance of an air-breathing propulsion system. Scramjet necessitates a combustor having an efficient fuel-air mixing and combustion of fuel with air at supersonic speeds without much pressure loss[3,4]. Many experimental and numerical analyses have been reported during the last few decades with respect to the characteristics of the complex flow field, resulting due to fuel-air mixing and combustion. Riggins [5,6], et al. observed that, the shock waves, incomplete mixing and viscous effects are the main factors leading to the thrust loss in supersonic combustors, though these effects aid mixing. Strut injectors offer a possibility for parallel injection without causing much blockage to the incoming stream of air and also fuel can be injected at the core of the stream. Tomioka[7,8] et al. observed the effects of staged injection from struts. Gerlinger and Bruggemann[9] conducted a numerical investigation of hydrogen injection from strut to foresee the effects of lip thickness of the injector in mixing. They concluded that, the increase in lip thickness caused an increase in mixing layer due to the raised diffusivity associated with it which did not have much effect on mixing efficiency.

The air flow entering a combustor will remain supersonic after the optimal compression when the flight speed is higher than a certain value and that time the efficiency of the engine will decrease with a further compression. Therefore, the combustion has to take place under the supersonic flow condition. The efficiency of heat supply to the combustion chamber based on the analysis of literature data on combustion processes in a confined high-velocity and high-temperature flow for known initial parameters is considered which was given by Mr. P. K. Tretyakov [10].

**Manuscript received on April 26, 2012.**

**Sukanta Roga**, M.Tech.student in Thermal Engineering, Department of Mechanical Engineering, N.I.T Silchar, Assam, India, Mob. No.:+91-9401926567, (e-mail: sukanta.me42@gmail.com).

**K.M.Pandey**, Professor, Department of Mechanical Engineering,N.I.T Silchar, Assam, India,Mob. No.:+91-9435173130, (e-mail: kmpandey2001@yahoo.com).

**A.P.Singh**, Lecturer,Department of Mechanical Engineering, N.I.T Silchar, Assam, India, Mob. No.:+91-8822925313, (e-mail: hello2apsingh@gmail.com).

# Computational Analysis of Supersonic Combustion using Wedge-Shaped Strut Injector with Turbulent Non-Premixed Combustion Model

The process efficiency is characterized by the combustion completeness and total pressure losses.

The main attention is paid to the local intensity of heat release, which ascertains together with the duct geometry, techniques for flame initiation and stabilization, injection techniques, quality of mixing the fuel with oxidizer and the gas-dynamic flow regime. The study of supersonic combustion of hydrogen has been conducted by Shigeru Aso and Arifnur Hakim et al. [11] and using a reflected-type shock tunnel which generated a stable supersonic air flow of Mach 2 with the total temperature of 2800K and the total pressure of 0.35 MPa.

As the flight Mach number goes above the range of 3 to 6, the use of supersonic combustion allows higher specific impulse. These elevated temperatures are sufficient enough to melt down most of the known materials [12]. The increased temperatures can cause the disassociation of the combustion products, thus in-turn limiting the temperature rise and thereby reducing thermal efficiency. The near-stagnation pressure resulting from slowing down high speed supersonic flow to subsonic conditions can advance the burner inlet pressure. As inlet pressure of burner is the highest pressure within a scramjet combustor, elevating this pressure will cause the mechanical and thermal loads to increase. This will call for an increased weight so as to withstand the structural loads. Thus, the structural integrity of the vehicle dictates the supersonic combustion past Mach 6. Hence, to obtain higher flight Mach numbers, the heat release due to combustion should take place at supersonic velocities. This proves that supersonic combustion ramjet or scramjet is an essential and efficient solution for hypersonic flight applications [13].

Supersonic combustion data obtained at the low static temperatures annexation for an efficient scramjet engine are reviewed by T. Cain and C. Walton [14]. The main attention is focused at the methods by which the fuel was ignited and combustion maintained which is particularly common for supersonic combustion experiments and many examples are found in the literature of experiments conducted with inlet temperatures much higher than practical in flight. A numerical study of mixing and combustion enhancement has been performed by Peter Gerlinger and Peter Stoll et al. [15] for a Mach 2. Due to the extremely short residence time of the air in supersonic combustors, an efficient (rapid and with small losses in total pressure) fuel/air mixing is hard to achieve.

K.Kumaran and V.Babu [16] observes that, the effect of chemistry models on the predictions of supersonic combustion of hydrogen in a model combustor. The calculations show that, the multi step chemistry predicts higher and wider spread heat release than what is predicted by single step chemistry. A Lagrangian model of turbulent combustion in supersonic flows has been used in conjunction with an efficient RANS-AMA strategy to simulate both reactive and non-reactive turbulent supersonic jet engines. Liquid hydrocarbon supersonic combustion has been experimentally investigated by C. Gruenig\* And F [17]. Kerosene was burnt in a steady, vitiated Mach 2.15 of air flow of a model scramjet combustor. The fuel is injected into the supersonic air stream by means of pylons. By the addition of small amounts of hydrogen to the kerosene the liquid fuel jet is dispersed and a fine spray produced. However, this

additional fuel jet dispersion is not necessary for the supersonic combustion if the fuel is injected normally into the cross flow. P.Manna & D.Chakraborty et al.[18] shows that, the reacting/low field of hydrogen-air combustion behind a backward facing step in a constant area combustor which is simulated numerically by solving three-dimensional Navier-Stokes equations along with k-epsilon turbulence model and fast rate chemistry. Investigation of kerosene combustion in a Mach 2.5 flow was carried out using a supersonic combustor model with cross-section area of (51 × 70) mm and different integrated fuel injector/flame-holder cavity modules is done. The experiments with pure liquid atomization and with effervescent atomization were characterized and compared. Within the same operational conditions, comparison of the measured static pressure distributions along the combustor also shows that, the effervescent atomization usually guides to better combustion performance than the use of pure liquid atomization.

## II. MATERIAL AND METHODS

### A. Physical model

A mathematical model comprises equations relating the dependent and the independent variables and the relevant parameters that describe some physical phenomenon. In general, a mathematical model consists of differential equations that govern the behavior of the physical system, and the associated boundary conditions which is shown in figure1.

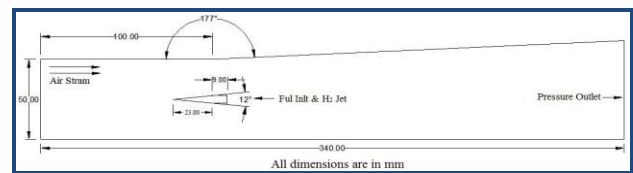


Fig.1. Physical model of Non-premixed supersonic combustor

### B. Governing equations

The advantage of employing the complete Navier-Stokes equations extends not only the investigations that can be carried out on a wide range of flight conditions and geometries, but also in the process the location of shock wave, as well as the physical characteristics of the shock layer, can be exactly determined. We begin by describing the three-dimensional forms of the Navier-Stokes equations below. Note that the two-dimensional forms are just simplification of the governing equations in the three dimensions by the omission of the component variables in one of the co-ordinate directions. Neglecting the presence of body forces and volumetric heating, the three-dimensional Navier-Stokes equations are derived as [19]:

Continuity equation:

$$\frac{\partial \rho}{\partial t} + \frac{\partial(\rho u)}{\partial x} + \frac{\partial(\rho v)}{\partial y} + \frac{\partial(\rho w)}{\partial z} = 0 \quad (1)$$

X-momentum equation:

$$\frac{\partial(\rho u)}{\partial t} + \frac{\partial(\rho uu)}{\partial x} + \frac{\partial(\rho uv)}{\partial y} + \frac{\partial(\rho wu)}{\partial z} = \frac{\partial \delta_{xx}}{\partial x} + \frac{\partial \tau_{yx}}{\partial y} + \frac{\partial \tau_{zx}}{\partial z} \quad (2)$$

Y-momentum equation:

$$\frac{\partial(\rho v)}{\partial t} + \frac{\partial(\rho uv)}{\partial x} + \frac{\partial(\rho vv)}{\partial y} + \frac{\partial(\rho vw)}{\partial z} = \frac{\partial \tau_{xy}}{\partial x} + \frac{\partial \sigma_{yy}}{\partial y} + \frac{\partial \tau_{zy}}{\partial z} \quad (3)$$

Z-momentum equation:

$$\frac{\partial(\rho w)}{\partial t} + \frac{\partial(\rho uw)}{\partial x} + \frac{\partial(\rho vw)}{\partial y} + \frac{\partial(\rho ww)}{\partial z} = \frac{\partial \tau_{xz}}{\partial x} + \frac{\partial \tau_{yz}}{\partial y} + \frac{\partial \sigma_{zz}}{\partial z} \quad (4)$$

Energy equation:

$$\frac{\partial(\rho E)}{\partial t} + \frac{\partial(\rho uE)}{\partial x} + \frac{\partial(\rho vE)}{\partial y} + \frac{\partial(\rho wE)}{\partial z} = \frac{\partial(u\sigma_{xx} + v\tau_{xy} + w\tau_{xz})}{\partial x} + \frac{\partial(u\tau_{yx} + v\sigma_{yy} + w\tau_{yz})}{\partial y} + \frac{\partial(u\tau_{zx} + v\tau_{zy} + w\sigma_{zz})}{\partial z} + \frac{\partial(k\frac{\partial T}{\partial x})}{\partial x} + \frac{\partial(k\frac{\partial T}{\partial y})}{\partial y} + \frac{\partial(k\frac{\partial T}{\partial z})}{\partial z} \quad (5)$$

Assuming a Newtonian fluid, the normal stress  $\sigma_{xx}$ ,  $\sigma_{yy}$  and  $\sigma_{zz}$  can be taken as combination of the pressure  $p$  and the normal viscous stress components  $\tau_{xx}$ ,  $\tau_{yy}$ , and  $\tau_{zz}$  while the remaining components are the tangential viscous stress components whereby  $\tau_{xy} = \tau_{yx}$ ,  $\tau_{xz} = \tau_{zx}$ , and  $\tau_{yz} = \tau_{zy}$ . For the energy conservation for supersonic flows, the specific energy,  $E$  is solved instead of the usual thermal energy  $H$  applied in sub-sonic flow problems. In three dimensions, the specific energy  $E$  is repeated below for convenience:

$$E = e + \frac{1}{2}(u^2 + v^2 + w^2) \quad (6)$$

It is evident from above that the kinetic energy term contributes greatly to the conservation of energy because of the high velocities that can be attained for flows, where  $Ma > 1$ . Equations (1)-(6) represent the form of governing equations that are adopted for compressible flows. The solution to the above governing equations nonetheless requires additional equations to close the system. First, the equation of state on the assumption of a perfect gas unempoyed, that is,

$$P = \rho RT$$

Where,  $R$  is the gas constant.

Second, assuming that the air is calorically perfect, the following relation holds for the internal energy:

$$e = CvT,$$

Where,  $Cv$  is the specific heat of constant volume. Third, if the Prandtl number is assumed constant (approximately 0.71 for calorically perfect air), the thermal conductivity can be evaluated by the following:

$$k = \frac{\mu C_p}{Pr}$$

The Sutherland's law is typically used to evaluate viscosity  $\mu$ , which is provided by:

$$\mu = \mu_0 \left( \frac{T}{T_0} \right)^{1.5} \frac{T_0 + 120}{T + 120} \quad (7)$$

Where  $\mu_0$  and  $T_0$  are the reference values at standard sea level conditions

Generalized form of Turbulence Equations is as follows:

$$(k) \frac{\partial k}{\partial t} + \frac{\partial(uk)}{\partial x} + \frac{\partial(vk)}{\partial y} + \frac{\partial(wk)}{\partial z} = \frac{\partial}{\partial x} \left[ \frac{V_T \partial k}{\sigma_k \partial x} \right] + \frac{\partial}{\partial y} \left[ \frac{V_T \partial k}{\sigma_k \partial y} \right] + \frac{\partial}{\partial z} \left[ \frac{V_T \partial k}{\sigma_k \partial z} \right] + (S_k = P - D)$$

$$(e) \frac{\partial \epsilon}{\partial t} + \frac{\partial(u\epsilon)}{\partial x} + \frac{\partial(v\epsilon)}{\partial y} + \frac{\partial(w\epsilon)}{\partial z} = \frac{\partial}{\partial x} \left[ \frac{V_T \partial \epsilon}{\sigma_k \partial x} \right] + \frac{\partial}{\partial y} \left[ \frac{V_T \partial \epsilon}{\sigma_k \partial y} \right] + \frac{\partial}{\partial z} \left[ \frac{V_T \partial \epsilon}{\sigma_k \partial z} \right] + (S_\epsilon = \frac{\epsilon}{k} (C_{\epsilon 1} P - C_{\epsilon 2} D))$$

Where,

$$P = 2v_T \left[ \left( \frac{\partial u}{\partial x} \right)^2 + \left( \frac{\partial v}{\partial y} \right)^2 + \left( \frac{\partial w}{\partial z} \right)^2 \right] + v_T \left[ \left( \frac{\partial u}{\partial y} + \frac{\partial v}{\partial x} \right)^2 + \left( \frac{\partial v}{\partial z} + \frac{\partial w}{\partial y} \right)^2 + \left( \frac{\partial w}{\partial x} + \frac{\partial u}{\partial z} \right)^2 \right]$$

And  $D = \epsilon$ .

### III. COMPUTATIONAL MODEL PARAMETER

#### A. Geometry and mesh generation

Mesh generation was performed in a Fluent pre-processing program called Gambit. The current model is wedge-shaped strut injector with non-premixed combustion as shown in figure 2. The boundary conditions are such that, the air inlet and fuel inlet surfaces are defined as velocity inlets and the outlet is defined as pressure outlet. Recent research has revealed that perhaps the numerical model will improve if the air inlet is defined as pressure inlet and the fuel inlet is defined as a mass flow inlet [20]. In this particular model the walls of the combustor duct do not have thicknesses. The domain is completely contained by the combustor itself; therefore there is actually no heat transfer through the walls of the combustor.

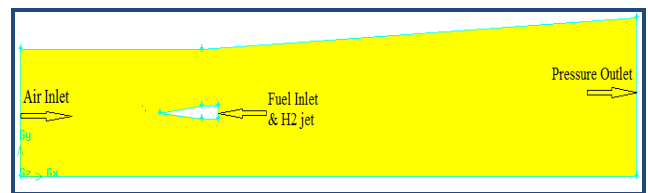


Fig.2. Two dimensional model of strut injector

#### B. Geometry and grid arrangement

The geometry of 2-D computational domain was considered for the simulation of supersonic combustion. The grid arrangement of two dimensional non-premixed combustion model is shown in figure 3.

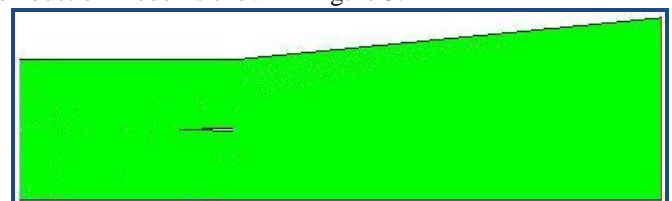


Fig.3. Grid refinement of supersonic combustor

#### C. Numerical methodology

The model supersonic combustor considered in the present work is show in figure 2. The combustor is 0.340 m long, 0.05 m at air inlet and 0.06258 m at pressure outlet. Vitiated air enters through the inlet with hydrogen being injected through the strut injector. The Mach number at inlet is 2 and stagnation temperature and static pressure for Vitiated air are 1495K and 1 bar respectively. Fuel is injected from the base which located at nozzle exit. The inlet condition of the H2 is considered as mass flow



rate at 1 bar. In addition 2ddp coupled with explicit model and turbulence and finite rate chemistry are also considered.

IV. BOUNDARY CONDITIONS

TABLE 1

EVANS ET AL.. [21] INFLOW CONDITIONS OF THE AIR STREAM AND THE HYDROGEN JET.

Sl. No.	Free stream conditions	Oxidizer	Fuel	Fuel Stream
1.	Mach number	2	1	0.03
2.	Temperature (K)	1495	251	
3.	Pressure (bar)	1	1	
4.	Velocity(m/s)	1510	2432	
5.	Mass fraction of H <sub>2</sub>	0	1	
6.	Mass fraction of N <sub>2</sub>	0.425	0	
7.	Mass fraction of O <sub>2</sub>	0.187	0	
8.	Mass fraction of H <sub>2</sub> O	0.388	0	

D. Approximations and idealizations

- The gas is compressible which obeying the real gas laws and
- The flow is considered to be in steady state which is non-adiabatic.

V. RESULTS AND DISCUSSION

The results from the numerical simulation for supersonic combustion using strut injector with non-premixed combustion model are discussed below:

A. Contours of static temperature

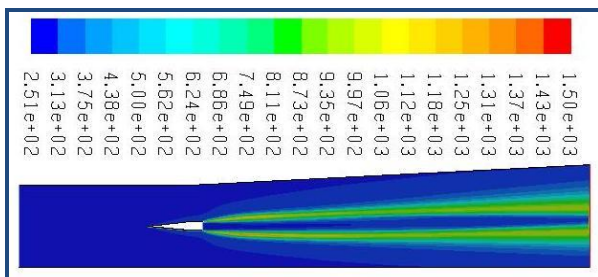


Fig.4: Contours of Static Temperature (k)

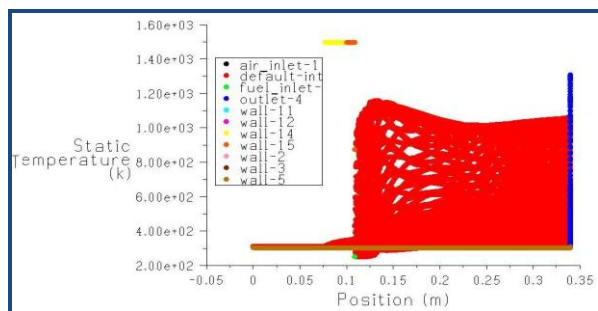


Fig.5: X-Y plot of Static Temperature

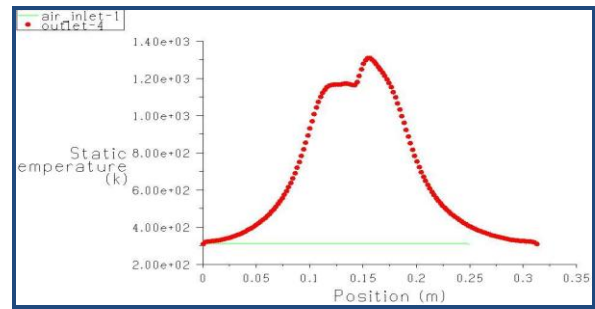


Fig.6: Static temperature distribution for air inlet and pressure outlet

The contour of static temperature of the resulting flow is shown in figure 4. It is observed from the figure 4 & figure 5 that, the maximum temperature of 1495 k occurred in the recirculation areas which are produced due to shock wave interaction and fuel jet losses concentration and the temperature is decrease slightly along the axis. The blue streamlines in the image representing the pressure gradients and hydrogen injection for the shocks. Due to combustion, the recirculation region behind the wedge shaped becomes larger as compared to mixing case which acts as a flame holder for the hydrogen diffusion flame. The leading edge shock reflected off the upper and lower combustor walls makes the setting of combustion when it hits the wake in a region where large portions of the injected fuel have been mixed up with the air. The recompression shocks at the upper and lower wedge corners become much weaker than mixing case. The shear layers at the base of the wedge becomes more pronounced with combustion due to the fact that continuous ignition occurs within these shear layers. Figure 5 shows that the profile between the static temperature and the position of the combustion on all conditions such as air inlet, fuel inlet, pressure outlet, default interior and all walls, where the figure 6 shows that the profile between static temperature and the position of the combustion on air inlet and pressure outlet.

B. Contours of total temperature

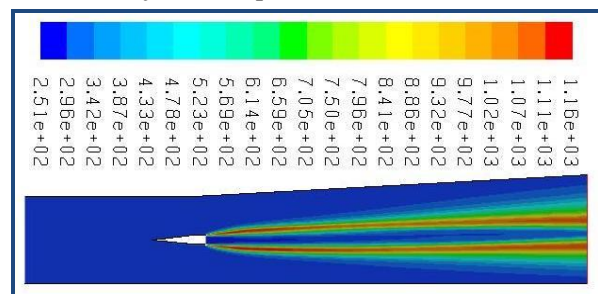


Fig.7: Contours of Total Temperature (k)

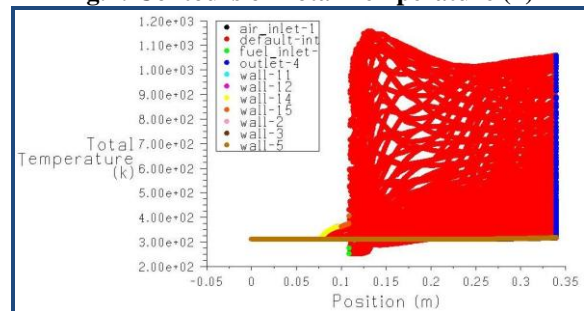
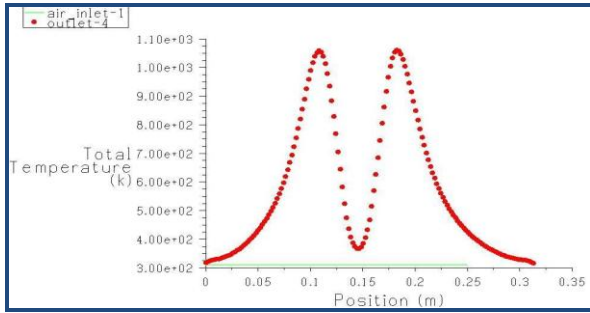
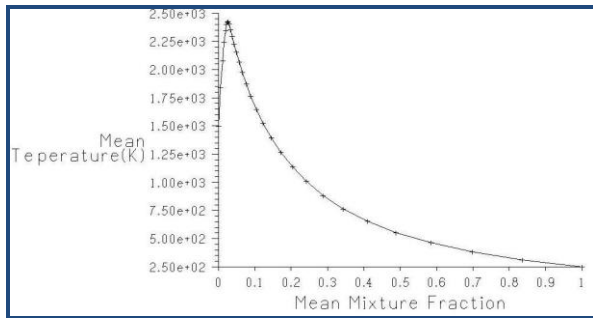


Fig.8: X-Y plot of Total Temperature



**Fig.9: Total temperature distribution for air inlet and pressure outlet.**



**Fig.10: Contours of Mean Temperature (k)**

The contour of total temperature of the resulting flow is shown in figure 7. It is observed from the figure 7 and figure 8 that, the maximum temperature of 1158.601 k occurred in the recirculation areas which are produced due to shock wave interaction and fuel jet losses concentration and the temperature is decrease slightly a value of 251 along the axis. The blue streamlines in the image representing the pressure gradients and hydrogen injection for the shocks. Due to combustion, the recirculation region behind the wedge becomes larger as compared to mixing case which acts as a flame holder for the hydrogen diffusion flame. The leading edge shock reflected off the upper and lower combustor walls makes the setting of combustion when it hits the wake in a region where large portions of the injected fuel have been mixed up with the air. The recompression shocks at the upper and lower corners become much weaker than mixing case. The shear layers at the base of the wedge becomes more pronounced with combustion due to the fact that continuous ignition occurs within these shear layers. The figure 8 shows that the profile between the total temperature and the position of the combustion on all conditions such as air inlet, fuel inlet, pressure outlet, default interior and all walls, where the figure 9 shows that the profile between the total temperature and the position of the combustion on air inlet and pressure outlet.

**C. Contours of density**

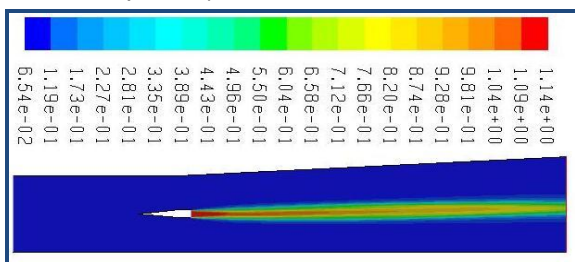


**Fig.11: Contours of density (kg/m3)**

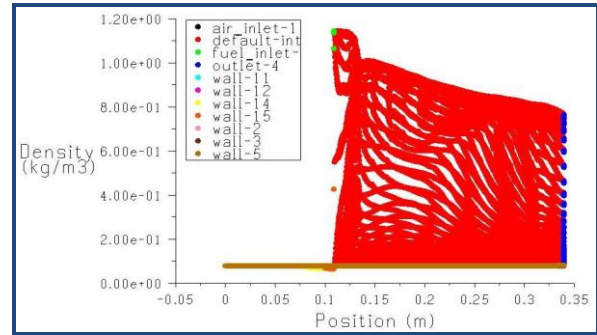


**Fig.12: X-Y plot of density (kg/m3)**

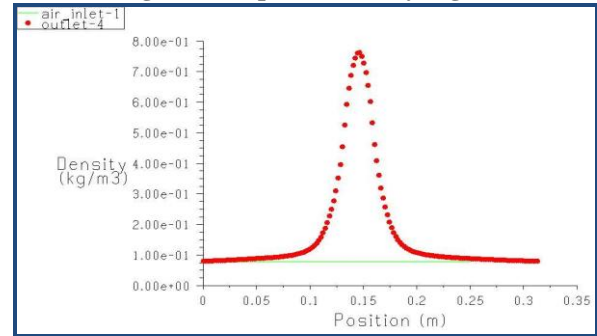


**Fig.13: Contours of density (kg/m3)**

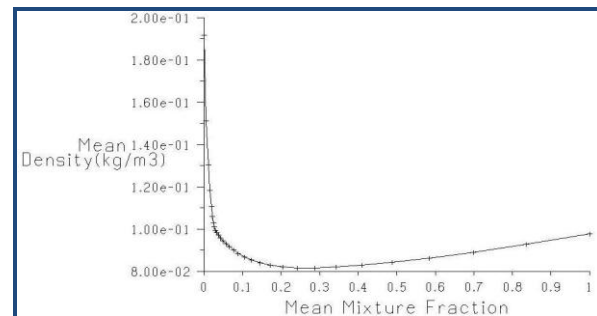


**Fig.14: Contours of mean density (kg/m3)**

The contours of density are shown in figure 11. From the figure 11 it is observed that, after the combustion the maximum density is occurred in the tip of the fuel inlet as 1.143 kg/m<sup>3</sup> where the minimum density is 0.0653 kg/m<sup>3</sup>. The Figure 12 shows that the profile between the density and the position of the combustion on all conditions such as air inlet, fuel inlet, pressure outlet, default interior and all walls, where the figure 13 shows that the profile between the density and the position of the combustion on air inlet and pressure outlet.

**D. Contours of mass fraction of H2**

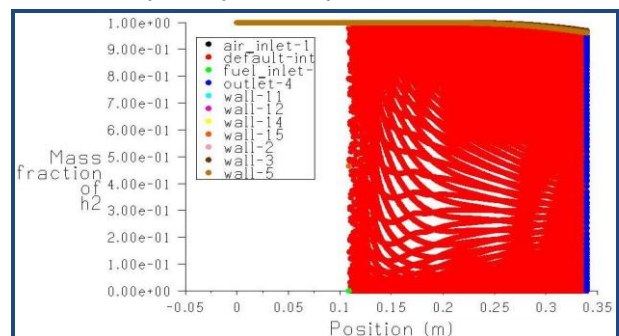


**Fig.15: X-Y Mass fraction of H2**

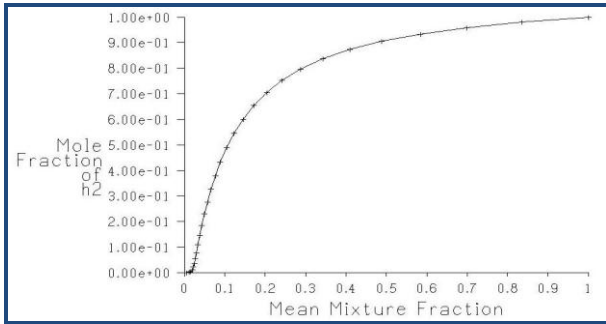


Fig.16: Contours of Mole fraction of H2

The contour of H<sub>2</sub> Mass fraction plot for the flow field downstream of the injector is shown in the figure 15. Low-velocity regions could be identified along the path of progress of the hydrogen jet. Alternate compression and expansion took place for the jet and was not enough to disorder the flow field much in the region near to the jet outlets. But the shock wave or expansion wave reflections interfered with the upcoming jet and localized low velocity regions were produced. Though, these regions are responsible for pressure loss of the jet, certainly enhanced the mixing and reaction. Lip height plays an important role in mixing enhancement. Figure 15 shows that the profile between the Mass fraction of H<sub>2</sub> and the position of the combustion on all conditions such as air inlet, fuel inlet, pressure outlet, default interior and all walls.

E. Contours of mass fraction of N<sub>2</sub>

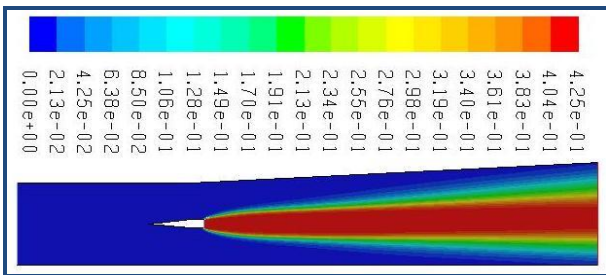


Fig.17: Contours of Mass fraction of N2

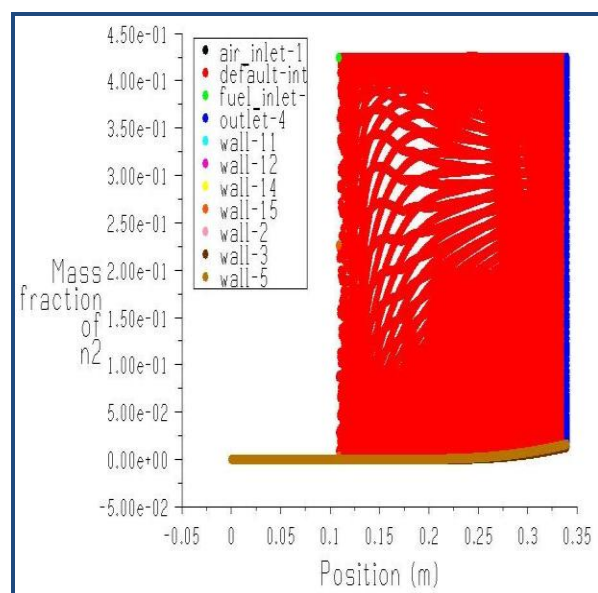


Fig.18: X-Y Mass fraction of N2

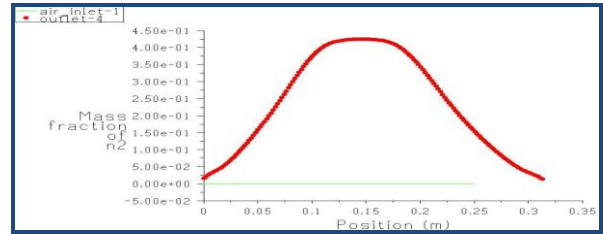


Fig.19: Contours of Mass fraction of N2 for air inlet and pressure outlet.

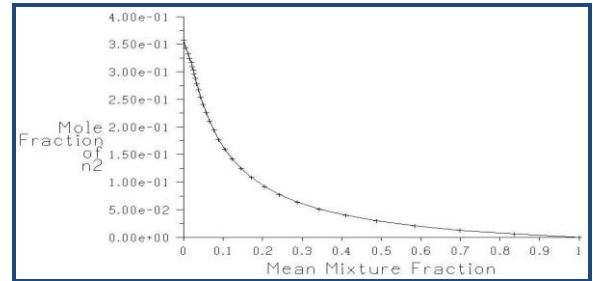


Fig.20: Contours of Mole fraction of N2

The contour of N<sub>2</sub> Mass fraction for the flow field downstream of the injector is shown in the figure 17. The major ratio of the N<sub>2</sub> to the O<sub>2</sub> is 3.76. When air supplies the O<sub>2</sub> in a combustion reaction, therefore every mole of O<sub>2</sub> is accompanied by 3.76 moles of N<sub>2</sub>. From the figure 12 it is observed that, the maximum mass fraction of N<sub>2</sub> is 0.425 which is found out after combustion. Figure 18 shows that the profile between the mass fraction of N<sub>2</sub> and the position of the combustion on all conditions such as air inlet, fuel inlet, pressure outlet, default interior and all walls, where the figure 19 shows that the profile between the mass fraction of N<sub>2</sub> and the position of the combustion on air inlet and pressure outlet.

F. Contours of mass fraction of O<sub>2</sub>

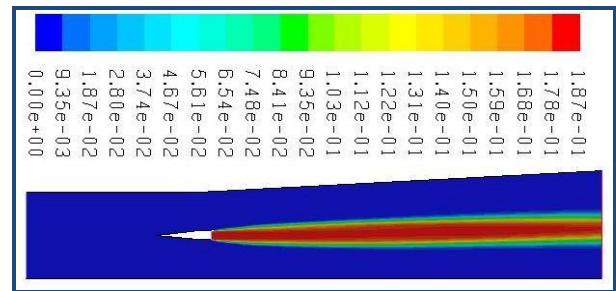


Fig.21: Contours of Mass fraction of O2

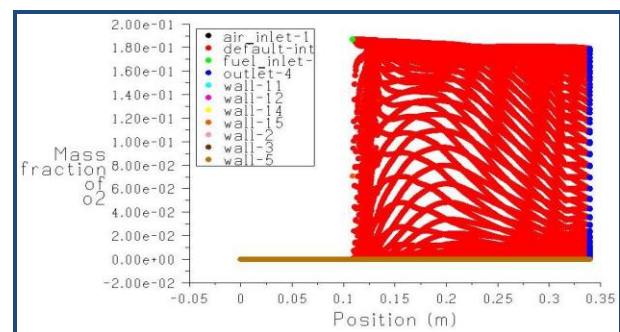
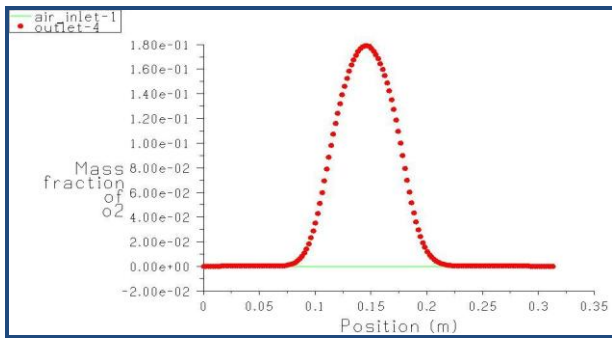


Fig.22: X-Y Mass fraction of O2



**Fig.23: Contours of Mass fraction of O2 for air inlet and pressure outlet**

The contour of O<sub>2</sub> Mass fraction for the flow field downstream of the injector is shown in the figure 21. Oxygen is increased in every combustion reaction in combustion applications and air provides the required oxygen. All components other than air collected together with nitrogen. In air 21% of oxygen and 79% of nitrogen are present on a molar basis. From the figure 21 it is observed that, the maximum mass fraction of O<sub>2</sub> is 0.187 which is found out after combustion. Figure 22 shows that the profile between the mass fraction of O<sub>2</sub> and the position of the combustion on all conditions such as air inlet, fuel inlet, pressure outlet, default interior and all walls, where the figure 23 shows that the profile between the mass fraction of O<sub>2</sub> and the position of the combustion on air inlet and pressure outlet.

**G. Contours of mass fraction of H2O**

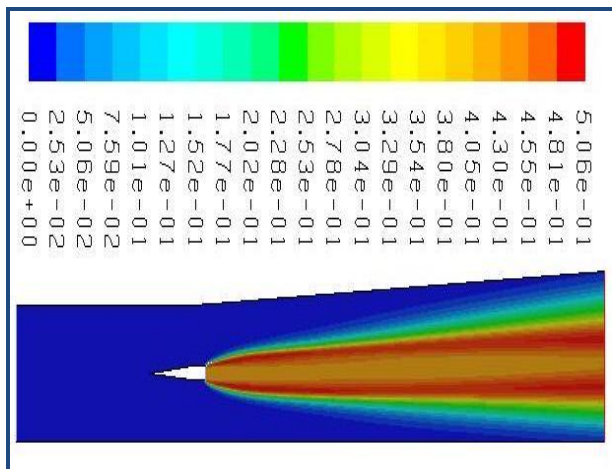


**Fig.24: Contours of Mass fraction of H2O**

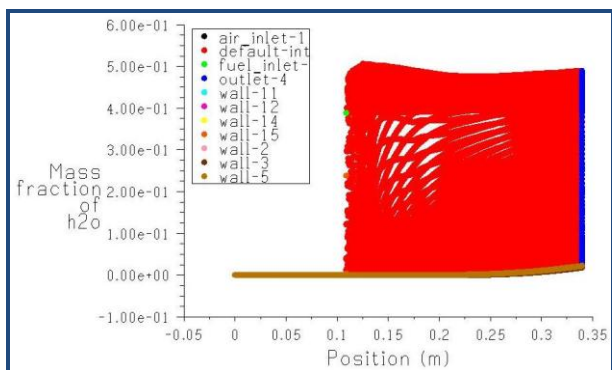


**Fig.25: X-Y Mass fraction of H2O**

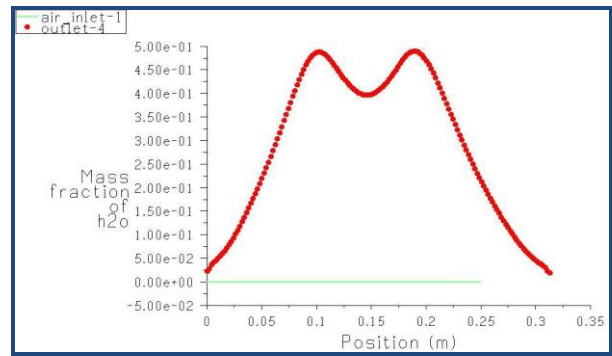


**Fig.26: Contours of Mass fraction of H2O for air inlet and pressure outlet**

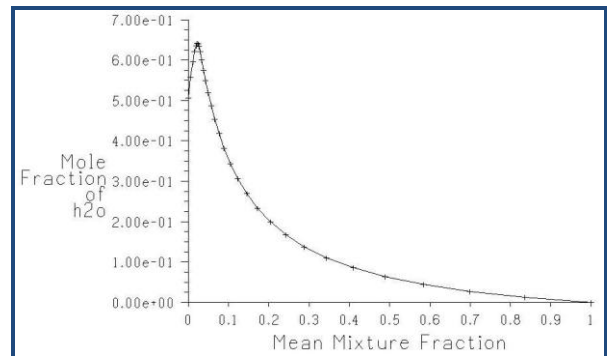


**Fig.27: Contours of Mole fraction of H2O**

The contour of water Mass fraction for the flow field downstream of the injector is shown in the figure 24. From the figure 24 is observed that, water concentration is found to be maximum value of 0.506 in the shear layer formed between the two streams of flow and the low-velocity recirculation regions within the core of the upcoming jet. Typically, when dealing the chemical reaction, it's important to remember that mass is conserved, so the mass of product is same as the mass of reactance. Even though the element exists in different the total mass of each chemical element must be same on the both side of equation. Figure 25 shows that the profile between the mass fraction of H<sub>2</sub>O and the position of the combustion on all conditions such as air inlet, fuel inlet, pressure outlet, default interior and all walls, where the figure 26 shows that the profile between mass fraction of H<sub>2</sub>O and the position of the combustion on air inlet and pressure outlet.

**H. Contours of mass fraction of H2O2**

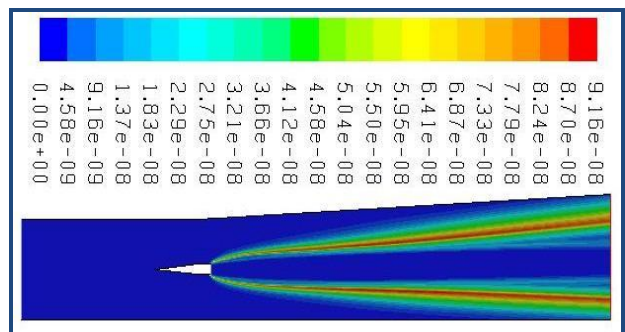


**Fig.28: Contours of Mass fraction of H2O2**

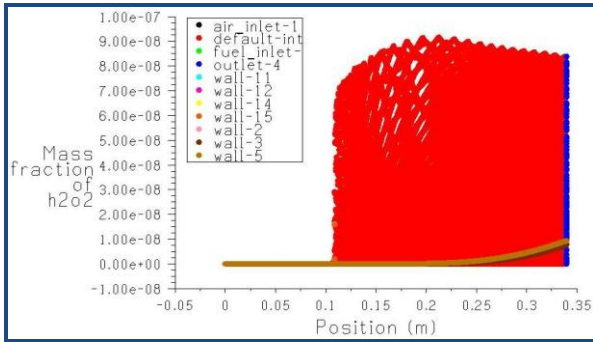


Fig.29: X-Y Mass fraction of H2O2

The contour of mass fraction of H<sub>2</sub>O<sub>2</sub> is shown in figure 28. From the figure 19 it is observed that, the maximum mass fraction of H<sub>2</sub>O<sub>2</sub> is 9.519e-08 which is found out after combustion, where the minimum value is 0. Figure 29 shows that the profile between the mass fraction of H<sub>2</sub>O<sub>2</sub> and the position of the combustion on all conditions such as air inlet, fuel inlet, pressure outlet, default interior and all walls.

I. Contours of mass fraction of OH

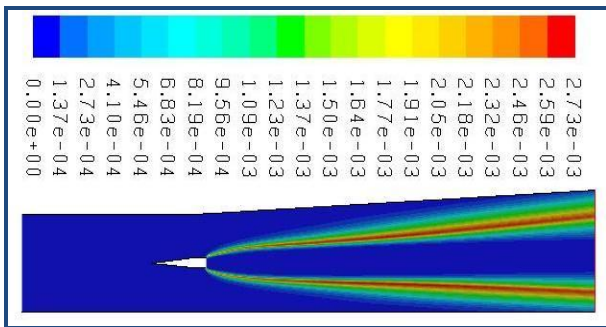


Fig.30: Contours of Mass fraction of OH

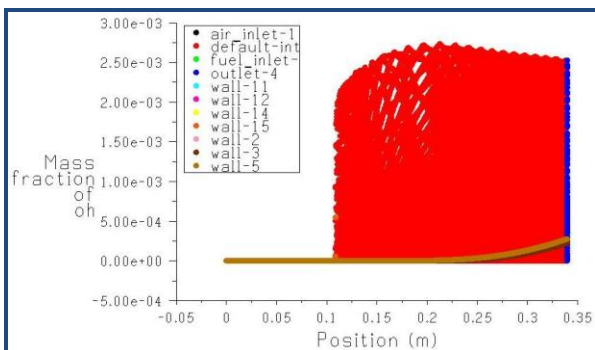


Fig.31: X-Y Mass fraction of OH

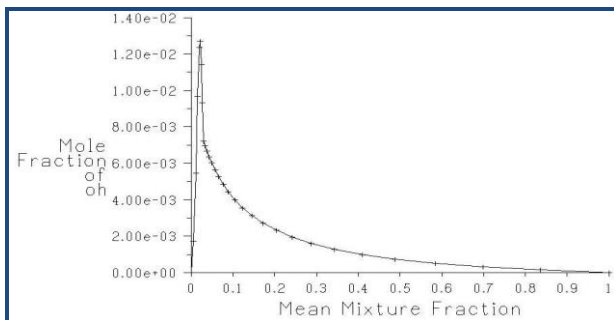


Fig.32: Contours of Mole fraction of OH

The contour of mass fraction of OH is shown in figure 30. From the figure 30 it is observed that, the maximum mass fraction of OH is 0.0027 which is found out after combustion,

where the minimum value is 0. Figure 31 shows that the profile between the mass fraction of OH and the position of the combustion on all conditions such as air inlet, fuel inlet, pressure outlet, default interior and all walls.

J. Contours of mean pdf mixture

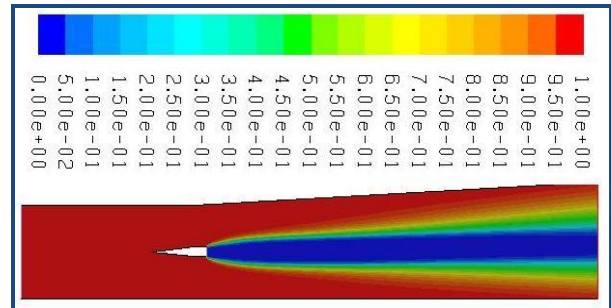


Fig.33: Contours of mean pdf mixture

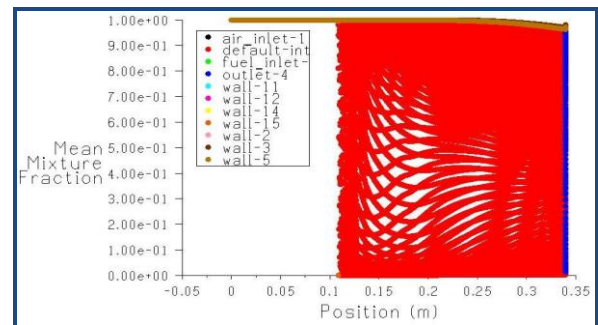


Fig.34: X-Y mean pdf mixture

The contour of mean pdf mixture is shown in figure 33. From the figure 33 it is observed that, the maximum value of mean pdf mixture is 1, where the minimum value is 0 which are found out after combustion. Figure 34 shows that the profile between the mean pdf mixture and the position of the combustion on all conditions such as air inlet, fuel inlet, pressure outlet, default interior and all walls.

The grid independent test is shown below:

Grid size	(original / adapted / change)
Cells	(114528 / 347601 / 233073)
Faces	(230133 / 698122 / 467989)
Nodes	(115605 / 350521 / 234916)

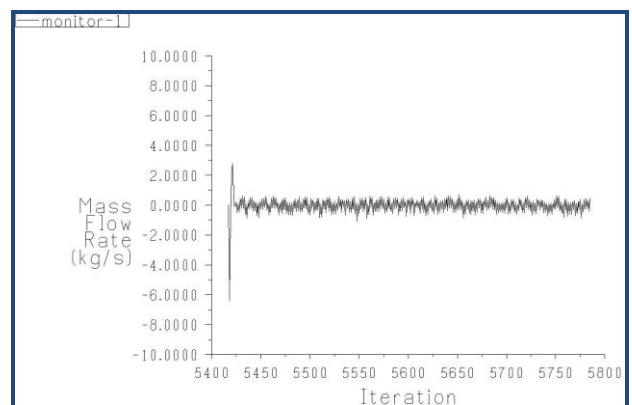


Fig.35: Convergence history of mass flow rate on air inlet, fuel inlet, pressure outlet and all walls

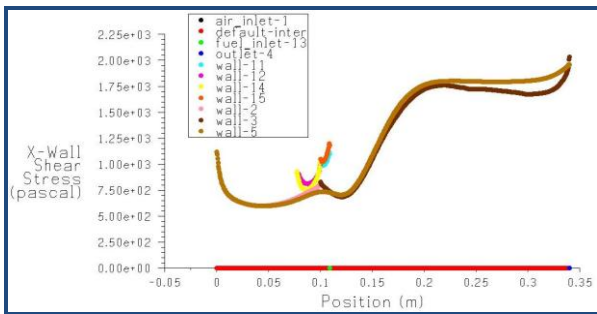


Fig.36: X-Wall shear stress (pascal) on air inlet, fuel inlet, pressure outlet and the walls

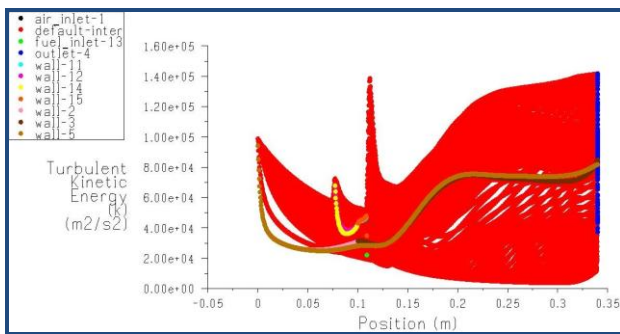


Fig.37: Turbulent Kinetic Energy (k) (m<sup>2</sup>/s<sup>2</sup>) on air inlet, fuel inlet, pressure outlet and the walls

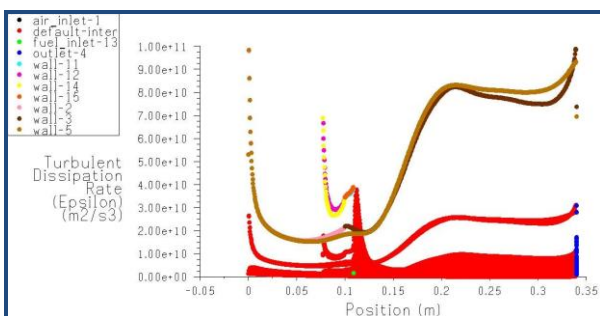


Fig.38: Turbulent Dissipation Rate ( $\epsilon$ ) (m<sup>2</sup>/s<sup>3</sup>) on air inlet, fuel inlet, pressure outlet and the walls

## VI. CONCLUSION

The computational analysis of 2D wedge-shaped strut injector was carried out with  $k-\epsilon$  turbulence model for exposing the flow structure of progress of hydrogen jet through the areas disturbed by the reflections of oblique shock. For that single step reaction kinetics has been used to model the chemistry. The  $k-\epsilon$  turbulence model also predicted the fluctuations in those regions where the turbulence is reasonably isotropic. From the maximum mass fraction of OH a very small amount of OH ( $2.70e-03$ ) was observed after combustion. By providing wedge-shaped strut injector, expansion wave is created which cause the proper mixing between the fuels and air which results in complete combustion. The major attention was paid to the local intensity of heat release which determines together with the duct geometry, techniques for flame initiation and stabilization, injection techniques and quality of mixing the fuel with oxidizer. The recirculations in the lip area of the injector and the shock reflections were well-captured. From the simulation it was concluded that the maximum temperature occurred in the recirculation areas which is produced due to shock wave-expansion, wave-jet

interaction and the fuel jet losses concentration and after passing successively through such areas, temperature decreased slightly along the axis.

## REFERENCES

1. Heiser, W.H., Pratt, D.T., *Hypersonic Airbreathing Propulsion*. 1994: AIAA Educational Series.
2. Andreadis, D. (2004) Scramjet Engines Enabling the Seamless Integration of Air and Space Operations.
3. Gruber, M.R. & Nejad, A.S. New supersonic combustion research facility. *J. Prop. Power*, 1995, **11**(5), 1080-83.
4. Riggins, D.W. & McClinton, C.R. "A computational investigation of flow losses in a supersonic combustor", AIAA Paper No. 90-2093, 1990.
5. Riggins, D.W.; McClinton, C.R. & Vitt, P.H. Thrust losses in hypersonic engines—Part 1: Methodology. *J. Prop. Power*, 1997, **13**(2).
6. Riggins, D.W.; McClinton, C.R. & Vitt, P.H., Thrust losses in hypersonic engines—Part 2: Applications. *J. Prop. Power*, 1997, **13**(2).
7. Tomioka, S.; Kanda, T.; Tani, K.; Mitani, T.; Shimura, T. & Chinzei, N. Testing of a scramjet engine with a strut in M8 flight conditions. AIAA Paper No. 98-3134, 1998.
8. Tomioka, S. Combustion tests of a staged supersonic combustor with a strut. AIAA Paper No. 98-3273, 1998.
9. Gerlinger, P. & Bruggemann, D. Numerical investigation of hydrogen strut injections into supersonic air flows. *J. Prop. Power*, 2000, **16**(1), 22-28.
10. P.K. Tretyakov "The Problems of Combustion at Supersonic Flow", West-East High Speed Flow Field Conference 19-22, November 2007.
11. Shigeru Aso, Arifnur Hakim, Shingo Miyamoto, Kei Inoue And Yasuhiro Tani "Fundamental Study Of Supersonic Combustion In Pure Air Flow With Use Of Shock Tunnel", Acta Astronautica 57 (2005) 384 – 389.
12. Andreadis, D. (2004) *Scramjets Integrate Air and Space*.
13. Bonanos, A.M., "Scramjet Operability Range Studies of an Integrated Aerodynamic-Ramp-Injector/Plasma-Torch Igniter with Hydrogen and Hydrocarbon Fuels", 2005: Blacksburg, VA.
14. T. Cain And C. Walton "Review Of Experiments On Ignition And Flame Holding In Supersonic Flow", Published By The America Institute Of Aeronautics And Astronautics, Rto-Tr-Avt-007-V2.
15. Peter Gerlinger, Peter Stoll 1, Markus Kindler, Fernando Schneider C, Manfred Aigner "Numerical Investigation Of Mixing And Combustion Enhancement In Supersonic Combustors By Strut Induced Streamwise Vorticity", Aerospace Science And Technology 12 (2008) 159–168.
16. K. Kumaran, V. Babu "Investigation of the effect of chemistry models on the numerical predictions of the supersonic combustion of hydrogen", Combustion And Flame 156 (2009) 826–841.
17. C. Gruenig\* And F. Mayinger "Supersonic Combustion Of Kerosene/H<sub>2</sub>-Mixtures In A Model Scramjet Combustor", Institute A For Thermodynamics, Technical University Munich, D-85747
18. P Manna, D Chakraborty "Numerical Simulation Of Transverse H<sub>2</sub> Combustion In Supersonic Airstream In A Constant Area Duct", Vol. 86, November 2005, ARTFC.
19. Jiyun tu, guan Heng yeoh and chaoqun liu. "Computational Fluid Dynamics", Elsevier Inc. 2008.
20. Fluent, Software Training Guide TRN-00-002.
21. Evans, J. S., Shexnayder Jr., C. J., and Beach Jr., H. L. (1978). Application of a Two-Dimensional Parabolic Computer Program to Prediction of Turbulent Reacting Flows. NASA Technical Paper 1169.
22. K.M. Pandey and A.P Singh, "Recent Advances in Experimental and Numerical Analysis of Combustor Flow Fields in Supersonic Flow Regime", *International Journal of chemical Engineering and Application*, Vol.-1, No.2, August 2010, ISSN-2010-0221, pp 132-137.
23. K.M. Pandey and A.P Singh, "Numerical Analysis of Supersonic Combustion by Strut Flat Duct Length with S-A Turbulence Model", *IACSIT International Journal of Engineering and Technology*, Vol.-3, No. 2, April 2010, pp 193-198.
24. K. M. Pandey and A. P. Singh, "Numerical Analysis of Combustor Flow Fields in Supersonic Flow Regime with Spalart-Allmaras and k- $\epsilon$  Turbulence Models" *IACSIT International Journal of Engineering and Technology*, Vol.3, No.3, June 2011, pp 208-214.

## Computational Analysis of Supersonic Combustion using Wedge-Shaped Strut Injector with Turbulent Non-Premixed Combustion Model

25. K.M. Pandey and A.P Singh, "CFD Analysis of Conical Nozzle For Mach 3 at Various Angles of Divergence With Fluent Software" *International Journal of chemical Engineering and Application* ,Vol.-1, No. 2, August 2010,ISSN- 2010-0221, pp 179-185.
26. K.M.Pandey and T.Sivasakthivel."CFD Analysis of Mixing and Combustion of a Scramjet Combustor with a Planer Strut Injector ", *International Journal of Enviromental Science and Development*, Vol. 2, No. 2, April 2011.
27. K.M. Pandey, A.P.Singh, "NUMERICAL SIMULATION OF COMBUSTION CHAMBER WITHOUT CAVITY AT MACH 3.12", *International Journal of Soft Computing and Engineering (IJSCE)* ISSN: 2231-2307, Volume-2, Issue-1, March 2012.
28. K.M. Pandey, S.K. Reddy K.K., "Numerical Simulation of Wall Injection with Cavity in Supersonic Flows of Scramjet Combustion", *International Journal of Soft Computing and Engineering (IJSCE)* ISSN: 2231-2307, Volume-2, Issue-1, March 2012.

### AUTHORS PROFILE



**Mr. Sukanta Roga** doing his M.Tech in Thermal Engineering under Mechanical Engineering Department from NIT Silchar, Assam, India from 2010. He has published one paper in IJSCE. His research interest areas are CFD, Fuzzy Logic Approach, Combustion and Gasification.  
Email: sukanta.me42@gmailcom



**Dr. K.M.Pandey** (Member IACSIT) did his B.Tech in 1980 from BHUIT Varanasi, India in 1980.He obtained M.Tech. in heat power in 1987 .He received PhD in Mechanical Engineering in 1994 from IIT Kanpur. He has published and presented more than 200 papers in International & National Conferences and Journals. Currently he is working as Professor of the Mechanical .Engineering Department,

National Institute of Technology, Silchar, Assam, India. He also served the department in the capacity of head from July 07 to 13 July 2010. He has alsoworked as faculty consultant in Colombo Plan Staff College, Manila, Philippines as seconded faculty from Government of India. His research interest areas are the following; Combustion, High Speed Flows, Technical Education, Fuzzy Logic and Neural Networks , Heat Transfer, Internal Combustion Engines, Human Resource Management, Gas Dynamics and Numerical Simulations in CFD area from Commercial Software"s. Currently he is also working as Dean, Faculty Welfare at NIT Silchar, Assam, India.  
Email:kmpandey2001@yahoo.com



**Mr. Aditya Pratap Singh** did his M.Tech in Thermal Engineering in 2008 from NIT Silchar. He has published and presented 42 papers in International & National Conferences and Journals. He has submitted his Ph.D Thesis in Department of Mechanical Engineering, National Institute of Technology, Silchar, Assam, India.. His research interest areas are the following; Gas Dynamics, Combustion, High Speed Flows,

Numerical Methods in Fluid Flow and Heat Transfer.  
Email:hello2apsingh@gmail.com